INSTITUTE OF PLASMA PHYSICS

NAGOYA UNIVERSITY

RESEARCH REPORT

NAGOYA, JAPAN

LAMINAR ELECTROSTATIC SHOCK WAVES GENERATED BY AN ION-BEAM*

H. Ikezi, T. Kamimura, M. Kako
and
K. E. Lonngren**

IPPJ-156 March 1973

Further communication about this report is to be sent to the Research Information Center, Institute of Plasma Physics, Nagoya University, Nagoya, Japan.

---

* Paper submitted to the Physics of Fluids.

**Permanent address: Department of Electrical Engineering, University of Iowa, Iowa City, Iowa, U.S.A.

Abstract

Strong laminar electrostatic shock waves have been experimentally observed when an ion-beam is injected into a collisionless plasma. The structure of the shock is qualitatively different from one with a trailing wave train. A density depression follows behind the shock front, and no trailing wave train due to wave dispersion is found. A significant amount of ions reflected from and transmitted through the shock front form a precursor. The critical Mach number above which no shock is formed is found to be 1.5. Numerical simulations reported here reproduce the experimental observations very well. An analysis based on the water-bag model accounts for the observed value of the critical ion-beam velocity which gives the critical Mach number. It also points out that the reflected ions play an essential role in the persistence of the shock.

I. INTRODUCTION

Formation of shock waves is one of the interesting nonlinear phenomena in a collisionless plasma.[1] When the density jump due to the shock is small compared with the background plasma density, the electrostatic shock wave is formed if the nonlinear "overtaking" is balanced by the dispersion of waves with large wavenumbers. This basic process has been demonstrated in recent experiments.[2-7] It has been pointed out, however, that a stationary state is achieved only when there exist energy dissipation mechanism in the system.[8-10] Two dissipation processes can be considered in a collisionless plasma: one is the dissipation due to the plasma turbulence at the shock transition[1,11] and the second is the reflection of the particles at the shock front.[8,10,12-16]

In this paper, we are concerned with laminar electrostatic shock waves in which the reflected ions play an essential role. A strong shock (the density jump at the shock transition is comparable with the background plasma density) is generated by the injection of an ion-beam into the plasma.[16] Experimental observations of the ion distribution in the phase plane give information on the behavior of the ions. The experimental conditions and methods are described in Section II. The experimental results, which are described in Section III, include: (i) the structure of the shock waves and (ii) the critical Mach numbers. We have carried out a numerical simulation of our experiments and describe these results in Section IV. Based on

the results of the experiments and of the numerical simulation, we theoretically analyze the structure of the shocks in Section V. The conclusions of the present study are summarized in Section VI.

II. EXPERIMENTAL CONDITIONS AND METHODS

The experiments is carried out in a double-plasma (DP) device.[17] Typical plasma parameters are: plasma density $n \simeq 10^8 - 10^9$ cm^{-3}; electron temperature $T_e \simeq 3$ eV; ion temperature $T_i \leq 0.2$ eV; argon gas pressure $p = (1 - 3) \times 10^{-4}$ Torr; electron Debye length $\lambda_D \sim 0.3$ mm; ion-thermal velocity $v_i \leq 7 \times 10^4$ cm/sec; and ion plasma frequency $\omega_{pi}/2\pi \sim 1$ MHz. The phase velocity of a small amplitude ion-acoustic wave is measured to be $c_{sE} = (2 - 2.5) \times 10^5$ cm/sec. The machine employed in the present experiment is the same one that is described in Ref.18. Two plasmas are partitioned by a negatively-biased fine mesh grid. The application of a positive potential ϕ_{ex} to one of the plasmas (driver plasma) injects an ion-beam into the other plasma (target plasma) when $\phi_{ex} > T_e/e$. It produces only a density perturbation in the target plasma when $\phi_{ex} < T_e/e$. The beam density n_b is 10^9 cm^{-3}.

The following two methods have been employed to generate the strong shocks: (i) An ion-beam is suddenly injected into the target plasma beginning from a certain time, say at $t = 0$ and the shock wave is generated from the leading edge of the beam. (ii) An ion-beam is continuously injected into the low target density background plasma ($n < n_b$).

Then, the beam energy is increased suddenly to a higher energy (faster velocity), say at t = 0. When the faster beam overtakes the slower beam, the shock wave is formed.

The density profile of the shock wave is monitored by observing the electron saturation current to a Langmuir probe. The ion energy distribution is measured with an electrostatic energy analyzer.[19] The evolution of the ion distribution in the energy-distance or the energy-time plane is displayed by employing a sampling technique.[20]

III. EXPERIMENTAL RESULTS

Propagation of the two kinds of shocks is shown in Fig.1. When the potential amplitude applied to the exciter ϕ_{ex} is small, the positive excitation signal increases the ion density near the grid. Figure 1(a) shows the nature of the compressional-wave propagation due to the applied potential ramp which is shown on the top trace. As the wave propagates, it steepens and is followed by a wave train that is dominated by dispersion.[3] The waveform of the wave train continuously changes. In Fig.1(b), the evolution of the shock generated by the continuous injection of an ion-beam is shown. The energy of the injected ion-beam is suddenly increased from 6 volts to 14 volts. The density jump in this case is more than 50% and the density pulse is relatively flat. The density of the background ions is much lower than that of the beam. We note that the width of the pulse increases slowly as it propagates and no trailing wave trains can be observed behind the shock. The

thickness of the shock front and the density depression are about 10 λ_D. A very small amplitude noise signal[21] (perturbed-to-unperturbed density ratio $\delta n/n_o \simeq 1 \times 10^{-2}$) is detected.

The ion distribution plotted in the energy-time plane at a fixed distance from the beam injection point is measured. In the case shown in Fig.2, the ion-beam is suddenly injected into the plasma starting at $t = 0$.
The beam density is nearly equal to the background ion density. The profile of the density shown on the top trace is essentially the same as that shown in Fig.1(b). The corresponding ion distribution is displayed on the bottom. In this figure, the dot density is proportional to the ion distribution and the various components are identified in the figure caption. Part (D) forms a foot in density (or precursor) in front of the shock as we can note on the top trace. The potential associated with the precursor induces a slight shift of the velocity of the background plasma (A).

The evolution of the ion distribution plotted in the energy-distance plane at fixed times after the beam energy is increased gives us more information about the shock wave. In Fig.3, a typical sequence of pictures for the same type of experiment as that shown in Fig.1 is illustrated. The ion-beam (3 eV) is continuously injected into a low density background plasma. The beam energy is suddenly increased to 7 eV at $t = 0$. We note that the high energy (velocity) beam starts overtaking the low energy beam at an

early stage of the evolution at 5 μsec. As the faster beam overtakes the slower one, excess ions accumulate. Although the electrons partially neutralize the ion charge, it is not complete because of the high electron temperature. As a result, a strong electric field is produced. This in turn modifies the ion distribution. The amplitude of the potential hump as measured by the Langmuir probe is sufficiently large to accelerate the background plasma and to decelerate the ion-beam, and let them merge with each other. The energy width of the ion distribution at the high density part is wider than that in the other region. However, this is not heating due to random processes but simply due to the fact that the two ion streams do not perfectly merge. Actually, no turbulent noise is observable in this part nor at the density jump. The contribution to the shock from the evolution of the low density background ions is observed to be weak. The shock structure is almost independent of the background ion density provided that the background density is small or the velocity separation between the beam and the background ions is large. It may be understood that the two experiments shown in Fig.2 and Fig.3 are essentially the same if we replace the background ions in the case of Fig.2 by the slower ion beam in the case of Fig.3.

Time resolved Langmuir probe curves show a slight anisotropy[13] in the low energy region of the electron distribution for the high density part of the shock structure. However, the Boltzmann distribution is still found to be a

good approximation to describe the electron distribution as observed by means of a Langmuir probe. The calculated mean e-e collision time is several micro-seconds. It should be noted however, that the electron mean-free-path is longer than the machine size.

The dependence of the shock structure on the ion-beam energy is shown in Fig.4. The beam ($n_b \simeq n$) is turned on at $t = 0$ and pictures are taken at $t = 19$ μsec. No ion-beam was injected when $t < 0$. When the potential step ϕ_{ex} is small a shock with a wave train [fig.1(a)] is observed. Since the spatial resolution of the ion energy analyzer is about 10 λ_D which is comparable with the width of the solitary wave pulse, the wave trains do not appear in the picture and only the velocity discontinuity is seen on the top picture. The density of the reflected ions is very small and is not seen in the picture. If the beam energy is increased [Fig.4(b)], a potential (density) depression appears behind the shock at $x = 3$ cm, and some reflected ions are observed. The amplitude of the wave train is very small. The Mach number just before this structure appears is 1.25. As shown in Fig.4(c), the width of the high density region is narrower for higher beam energy; i.e., the expansion velocity of the high density region is slower when the beam velocity is faster. The beam density in front of the shock is nearly equal to the injected beam density n_b and the background ion density n. It is found from a careful measurement of the ion distribution (not from a display like Fig.4) that the beam in front of the

shock consists mainly of the ions transmitted through the high density region, and the contribution of the reflected ions is small when v_b is large. The maximum density jump in the shock is observed to be 0.7 n when $n_b \simeq n$. As shown in Fig.4(d), the beam does not interact with the background ions, and no shock waves are formed if the beam energy is too high. Although the potential hump induced by the edge of the ion beam appears initially, it damps quickly in this case. Turbulent noise due to a two ion-stream instability grows. The unstable waves propagate obliquely to the beam direction. However their amplitude saturates at a very small level as noted before and the turbulence is unable to slow the directed beam velocity within the present experimental scale length, when the ion beam energy is high and there is no shock. The heating of the beam in the beam direction is also very small.

The observed Mach number M and the expansion velocity of the high density part 2 u are plotted in Fig.5(a) as a function of the beam velocity v_b. M increases and u decreases as v_b increases. It should be noted that the shock is formed even when $v_b > 2c_{sE}$ where the system is stable for the linear ion two-stream instability[22] in the beam direction. (The shock propagates in the beam direction and the observed structure of the shock is one-dimensional.) The shock wave disappears when $v_b = 3.0$ and $u = 0$. The corresponding upper critical Mach number is 1.5, when the density of the injected ion beam equals that of the background ions.

IV. NUMERICAL SIMULATIONS

To numerically simulate the experiments, we have employed the one-dimensional Vlasov-Poisson equations for ions and have assumed that the electrons are isothermal and obey the Boltzmann distribution. The method we used to solve the Vlasov equation is the same as that used by Sakanaka et al.[23] which is based on the fact that the distribution function is constant along the characteristics in phase space. Typical step sizes in space, velocity and time in the numerical computations are 0.7 λ_{De}, 0.05 c_s, and 0.5 ω_{pi}^{-1}, respectively. Numerical errors are checked by changing the above step sizes. The iteration method is applied for solving a finite difference scheme for Poisson's equation with the boundary condition $\phi(x = \pm L) = 0$. Here, L is much larger than the characteristic scale length of the shock.

In the reference frame moving with the average velocity of the two ion streams (center of mass frame), the initial condition for the laboratory experiment can be described by the ion distribution

$$f(v,x,t=0) = \frac{n_o}{(2\pi)^{1/2} v_i} \begin{cases} \exp[-(\frac{v + v_o}{v_i})^2] & \text{for } L > x > 0 \\ \exp[-(\frac{v - v_o}{v_i})^2] & \text{for } -L < x < 0, \end{cases} \tag{1}$$

provided that the densities of the two interacting ion streams are equal to each other. Therefore, the initial ion density is uniform in space. Here, $v_i = (2T_i/M)^{1/2}$ and

$2v_o$ is the velocity jump due to the application of a potential step to the driver plasma. The electron-to-ion temperature ratio is chosen to be 30.

The shock wave is generated from the above initial condition as shown in Fig.6. The ion beam velocity v_o/c_s equals 1.3. In this section, we define the ion-acoustic velocity by $c_s = (T_e/M)^{1/2}$, and x is measured in the center of mass frame. A stationary shock front with the thickness $D \simeq 7\lambda_D$ is found when $t > 30$. The shock transitions propagate both to the right and to the left so that the high density region expands. No trailing wave train appears behind the shock front. The density jump is approximately n_o. The velocity of the shock u in the center of mass frame is slower than v_o. In the experiment shown in Fig.1(b), for example, two ion-beams are moving to the right. Therefore, the density jump on the right-hand-side in the simulation corresponds to the shock front in the experiment and the one on the left-hand-side corresponds to the density depression.

From the evolution of the ion distribution in the phase plane, the building-up of the density jump is understood as follows: For small times t, the two ion beams overlap around $x = 0$ and generate an electric field which is positive for $x > 0$ and negative for $x < 0$ since the electrons do not completely shield the ion charge because of their finite temperature. If we consider the beam moving to the left (in Fig.7, it is moving downward), then the leading edge of the beam, already in the space $x < 0$,

is accelerated. The part staying in the space $x > 0$ is decelerated [Fig.7(b)] and accumulates more ions which in turn generate a stronger electric field. Although this process is similar to that of the two-stream instability, our shock wave is formed in the regime where the system is stable for the linear two-stream instability. We note here that the strong electric field is built up in the early stage of the evolution due to overlapping of the ion streams. The structures of the ion distribution shown in Fig.7(b,c) are essentially the same as those observed experimentally (Fig.3). The two ion-streams do not perfectly merge with each other in the high density region. The densities of the reflected and the transmitted ions are lower than those of the injected beam. This suggests that some of the injected ions are trapped in the high density region.

We find a discontinuity of the distribution at $v \simeq x/t$ in Fig.7(b,c). This discontinuity is observed to persist for a long time since the electric field is weak and no turbulence grows in the high density region except for a hole at $x = 0$. (The discontinuity may be smeared by diffusion in phase space due to numerical processes.) In the region $v > x/t$ the distribution consists of the ions supplied from $x < 0$. In the region $v < x/t$, it consists of the ions from $x > 0$. If we follow this discontinuity, we find that the beam in front of the shock consists mainly of the transmitted ions.

In Fig.8, the results of the simulations which corre-

spond to the experimental results shown in Fig.4 are presented. The beam velocity v_o is changed, keeping $\omega_{pi}t = 40$. When the beam velocity is small, $v_o/c_s = 0.4$, the density of the beam in front of the shock front (transmitted and the reflected ions) is small. For larger v_o, the above beam density increases and the width of the high density region decreases, i.e., u decreases. When $v_o/c_s = 1.5$, the two beams do not interact and no shock wave is formed.

Our main purpose in performing the simulations is to find the critical Mach numbers. In Fig.5(b) the Mach number M and the shock velocity u are plotted as a function of v_o. In the experiment, the background ions correspond to the ion stream which has the drift velocity $-v_o$ in the simulations. We therefore define the Mach number as $M = (u + v_o)/c_s$. In the limit of $v_o = 0$, u approaches $1.05\ c_s$ which is the ion-acoustic velocity $\{1 + (3T_i/T_e)\}^{1/2}c_s$ in the finite-ion-temperature plasma. The ion-acoustic velocity c_{sE} measured by the small-amplitude wave in the experiment corresponds to this quantity. If v_o is increased, then u decreases linearly and an extrapolation of the data points suggests $v_o/c_s = 1.65$ when $u = 0$. Although the simulation continues up to $\omega_{pi}t = 80$, no shock wave was formed when $v_o/c_s \geq 1.5$. We note that 1.65 is the critical value of v_o/c_s above which no shock wave could be generated. The critical Mach number observed in the simulation was 1.55 and agrees well with the experimental value of 1.5. The left-going shock has the velocity v_o-u

in the laboratory frame. If $v_o - u > 0$, then we find a density depression in the experimental geometry. We obtain a Mach number 1.3 from $v_o = u$ and the dependence of u on v_o.

V. ANALYSIS AND DISCUSSION

A. Analytical Description of the Shock

In this section, we analyze the structure of the shock employing the water-bag model.[24] The purpose of this analysis is to find the critical beam velocity which gives $u = 0$. We consider the structure of the ion distribution in the phase-plane sketched in Fig.9. The corresponding potential profile is shown at the bottom. Although the ion-beams consist of the reflected and the transmitted ions which extend a finite distance in the experiment, we assume that they extend to $x = \pm\infty$ so that the effects of the foot in the density and the potential are neglected. Hereafter, the normalized quantities;

$$\tau = \omega_{pi} t, \quad y = x/\lambda_D, \quad w = v/c_s \quad \text{and} \quad \psi = e\phi/T_e , \tag{2}$$

are used.

It is assumed that the structure in the right-half-plane ($y > 0$) moves to the right with the velocity s and that in the left-half-plane ($y < 0$) moves to the left with the velocity -s. We also assume that ψ takes its maximum value at $y = 0$ and vanishes at $y = \pm\infty$. The ion distribution function has a constant value h in the shaded region in

Fig.9 and vanishes elsewhere. The bounding curves I - IV evolve according to[25]

$$\frac{\partial w}{\partial \tau} + w \frac{\partial w}{\partial y} + \frac{\partial \psi}{\partial y} = 0 \ , \tag{3}$$

and

$$\frac{\partial^2 \psi}{\partial y^2} = \exp(\psi) - N \ , \tag{4}$$

where N is the ion density and the Boltzmann distribution has been assumed for electrons. The density is normalized by the density at $y = \infty$. Because of the symmetry of the system, we need calculate the distribution and the potential only in the right half plane $y > 0$ by introducing a variable $z = y - s\tau$ and connecting the two symmetric solutions at $y = 0$. Then the bounding curves and the potential are functions of z. Rewriting (3) and (4) in terms of z we have

$$-sw + \frac{1}{2} w^2 + \psi = A \ , \tag{5}$$

and

$$\frac{\partial^2 \psi}{\partial z^2} = \exp(\psi) - N \ , \tag{6}$$

where A is an integration constant to be determined by the boundary conditions. The velocity w_I which defines the bounding curve I is calculated to be

$$w_I = s - [(w_2 + s)^2 - 2\psi]^{1/2} \tag{7}$$

by imposing the condition $w_I = -w_2$ at $z = \infty$ where $\psi = 0$.

Curve II is calculated in the following way. From the symmetry of the system, w_{II} obeys the condition

$$w_{II}(y=0) = -w_I(y=0) \equiv w_i \ . \tag{8}$$

Employing Eq.(7), we have

$$w_{II} = s \pm [(w_i - s)^2 + 2\psi(y=0) - 2\psi]^{1/2} \tag{9}$$

The positive sign should be chosen when $w_i > s$ and the negative sign when $w_i < s$. In the present analysis, we treat the case $w_i > s$; otherwise the structure shown in Fig.9 cannot be formed. By putting $w_{III} = -w_1$ at $z = \infty$, the bounding curves III and IV are:

$$w_{III} = s - \{(w_1 + s)^2 - 2\psi\}^{1/2} \ , \tag{10}$$

and

$$w_{IV} = s + \{(w_1 + s)^2 - 2\psi\}^{1/2} \ . \tag{11}$$

Substitution of (7), (9), (10) and (11) into the expression for the ion density

$$N = h\{w_{II} - w_I - (w_{IV} - w_{III})\theta[(w_1 + s)^2 - 2\psi]\} \ , \tag{12}$$

gives an equation for ψ from Eq.(6). Here, $\theta(x)$ is the unit step function

$$\theta(x) = \begin{cases} 1, & x > 0 \\ 0, & x < 0 \ . \end{cases}$$

We now look for the shock solution of Eq.(6); i.e., ψ jumps from 0 to a positive constant value ψ_o when z changes from ∞ to $-\infty$.[26] Multiplying Eq.(6) by $\partial\psi/\partial z$ and integrating once, we find

$$\frac{1}{2}\left(\frac{\partial\psi}{\partial z}\right)^2 + V(\psi) = 0 \ , \tag{13}$$

where $V(\psi)$ is defined by

$$V(\psi) = -\int_o^{\psi} d\psi' [\exp(\psi') - N(\psi')] \ . \tag{14}$$

An integration constant which appeared in (13) has been determined by the fact that the electric field $\partial\psi/\partial z$ vanishes at $z = \infty$ where $\psi = 0$. If $\partial V/\partial\psi$ and $V = 0$ when $\psi = 0$ and $\psi = \psi_o$, then the shock potential profile is obtained [see Fig.10]. These conditions correspond to those of charge neutrality and no electric field at $z = \pm\infty$ and are explicitly written as

$$h(a + b - 2c) = 1 \tag{15}$$

$$h[(a^2 - 2\psi_o)^{1/2} + (b^2 - 2\psi_o)^{1/2}] = \exp(\psi_o) \ , \tag{16}$$

and

$$\frac{1}{3}h[a^3 + b^3 - 2c^3 - (a^2 - 2\psi_o)^{3/2} - (b^2 - 2\psi_o)^{3/2}]$$

$$= \exp(\psi_o) - 1 \ . \tag{17}$$

Here,

$$a^2 = (w_2 + s)^2, \quad b^2 = (w_i - s)^2 + 2\psi(y=0) ,$$

and

$$c^2 = (w_1 + s)^2 . \tag{18}$$

It is anticipated that ψ approaches ψ_o very quickly behind the shock, so that an approximation, $\psi(y=0) = \psi_o$, can be employed. (Errors of this approximation will be estimated later.) The set of equations (15), (16), and (17) is solved numerically for s, ψ_o and h. The dependence of s on the beam velocity w_o [$\equiv (w_1 + w_2)/2$] is plotted in Fig.5(c). Here, we have defined the velocity width $\Delta w \equiv w_2 - w_o = w_0 - w_1$. In order to compare with the experimental and the simulation results, the width is chosen to be $\Delta w = (2T_i/M)^{1/2}/c_s = 1/4$. As w_o is increased, s decreases and becomes zero when $w_o = 1.35$ which is in satisfactory agreement with the experimental value of 1.5 and with the simulation result of 1.65. In the limit of $\Delta w \to 0$, $w_o \cong 1.6$, when $s = 0$. Far upstream from the shock where $\psi = 0$, the input ion-beam density is $(a - c)h$ and the density which consists of reflected and transmitted ions is $(b - c)h$. The solution of (15), (16) and (17) shows that the density ratio $R \equiv (b - c)/(a - c)$ equals unity when $s = 0$ and the R decreases as w_o decreases. This fact qualitatively agrees with the experimental and simulation results.

The water-bag model fails in constructing the distribution shown in Fig.9 when w_o is small and w_i is smaller

than s; we therefore have to choose the negative sign in Eq.(9). The numerical solution shows that $w_i < s$ when $w_o < 0.72$ for $\Delta w = 1/4$. Only a solitary or oscillatory solution exists in this region. A realistic ion distribution, however, has a tail so that this drastic disappearance of the transmitted ions does not take place. In the above analysis, the reflected ions play an essential role. Without these reflected ions no shock solution can be obtained. The thickness of the shock front D is estimated from the relation

$$D = \frac{\psi_o}{(-2V_{min})^{1/2}} \tag{19}$$

to be about 5, i.e., $\sim 5\lambda_D$ in unnormalized units. Here, V_{min} is the minimum value of V. The meaning of Eq.(19) is illustrated in Fig.9.

To estimate the error of the approximation $\psi(y=0) = \psi_o$, V is expanded around $\psi = \psi_o$ in a Taylor series up to terms of $\frac{\partial^2 V}{\partial \psi^2}$. Because $\partial V/\partial \psi = 0$ when $\psi = \psi_o$, the expansion is

$$V = V(\psi_o) + \frac{1}{2} \frac{\partial^2 V}{\partial \psi^2} (\delta\psi)^2 , \tag{20}$$

where $\psi = \psi_o + \delta\psi$. From Eq.(13), the equation for $\delta\psi$ is

$$\frac{\partial(\delta\psi)}{\partial z} = \pm\left(-\frac{\partial^2 V}{\partial \psi^2}\right)^{1/2} \delta\psi . \tag{21}$$

The solution of (21) can be approximately written as

$$\delta\psi \simeq -\psi_o \exp[(-\frac{\partial^2 V}{\partial\psi^2})^{1/2}(y - y_o)] \ , \qquad (22)$$

when the argument in the exponent is larger than unity. Here, y_o is the position of the shock front and $(-\partial^2 V/\partial\psi^2)^{1/2}$ is calculated to be

$$(-\frac{\partial^2 V}{\partial\psi^2})^{1/2} = [1 + (a^2 - 2\psi_o)^{-1/2}(b^2 - 2\psi_o)^{-1/2}]^{1/2}\exp(\frac{1}{2}\psi_o) \qquad (23)$$

with the aid of Eq.(16). Since the right-hand-side of Eq.(23) is larger than unity, we find from Eq.(22) that the quantity $\delta\psi(y=0)$ which is neglected in our analysis is very small if $y_o >> 1$; i.e., if the width of the high density (potential) region is much wider than a Debye-length. The disconsinuity of the electric field at $y = 0$ due to the artificial connection of the two solutions for $y > 0$ and $y < 0$ is also found to be very small.

We note here that the above structure of the ion distribution is an example of a nonlinear equilibrium of the Bernstein-Green-Kruskal[27] type in each half space. However, the nonlinear equilibrium cannot be synthesized if we impose a realistic smooth ion distribution at $y = \pm\infty$ for the following reason. Let us consider the situation which is found in the experiments and the simulations, that of a potential hump which grows initially around $y = 0$ and the shock fronts propagate to both sides. In the high density part, the ions freely stream since the electric field is very weak. Because of the symmetry of the system, the ion

distribution f(w) is an evenfunction at y = 0. However $\partial f/\partial w$ is discontinuous at w = 0 except for the case when it vanishes. The discontinuity extends along the line y = $w\tau$ because the ions freely stream. The line y = $w\tau$ moves in the shock frame. This discontinuity is observed in the simulations, see Figs.7 and 8.

B. Discussion

Under the present method for the excitation of the shock, a small potential step applied to the driver plasma generates a shock with a trailing wave train (quasi-shock). In this case the density of the precursor is very small. For a higher potential step, the density of the transmitted and the reflected ions increases and a model for a laminar shock wave given by Sagdeev[10] does not apply.

Forslund and Freidberg[8] have reported that laminar shocks are possible between two critical Mach numbers. When the ions are cold, their lower critical Mach number is essentially the same as the one proposed by Sagdeev. Below this number, no reflected ions are present and above this number, the reflected ions play an essential role for the persistence of the shock. Although we do observe in our experiments, the two different types of shocks that are demonstrated in their numerical simulations, the transition from one to the other is continuous and no definite lower critical Mach number is found. (The water-bag model manifests definite ion-beam velocity w_o = 0.72 for Δw = 1/4, which introduces lower critical Mach number, since there

is no tail in the distribution.) The difference between the upper and the lower critical Mach number defined in Ref.8 is dominated by the potential jump due to the "foot". In the simulation of Forslund and Freidberg, the electrons are a one-dimensional collisionless fluid and they do not shield the reflected ions very well. Therefore, the resulting large potential jump at the foot modifies the ion trajectory and introduces a large range between the two critical Mach numbers. In the experiments reported here, the electrons are nearly isothermal and provide more shielding of the ions than the case of above numerical simulation. The experiments have demonstrated that the shift of the ion distribution due to the foot is very small, as a result the upper critical Mach number is not large.

Finally we note again that the turbulence excited by the ion two-stream instability saturates at a very small level. It does not slow nor heat the ion-beam within the distance $10(v_o/\omega_{pi})$ which is the value suggested by MacKee.[28] Under the present experimental conditions a turbulent shock would not be formed in spite of the two ion-streams generate turbulence.

VI. CONCLUSIONS

Strong laminar electrostatic shocks have been observed experimentally when an ion-beam is injected into a collisionless plasma. The features of the shock are as follows: (i) The density jump in the shock is comparable in magnitude with the background plasma density. (ii) No trailing wave

train due to wave dispersion is found. (iii) A density depression follows behind the shock front. (iv) A significant amount of ions reflected from and transmitted through the shock front are found. (v) The upper critical Mach number is 1.5 and the corresponding ion-beam velocity is 3 c_{sE} above which the beam does not interact with the background ions. (vi) The thickness of the shock front is about 10 λ_D.

Numerical simulations based on the Vlasov-Poisson equations have reproduced the above experimental results very well. An analysis using the "Water-Bag" Model of the above shock structure has accounted for the critical beam velocity reasonably well and has suggested that the reflected ions play an essential role in the persistence of the shock.

ACKNOWLEDGMENT

The authors appreciate the helpful discussions with Professor T. Taniuti. One author (KEL) participated in this research while on research leave from the University of Iowa at the Institute of Plasma Physics, Nagoya University and he was supported in part by the National Science Foundation.

REFERENCES

1. D. A. Tidman and N. A. Krall, Shock Waves in Collisionless Plasmas (Wiley, New York, 1971)
2. S. G. Alikhanov, V. G. Belan and R. Z. Sagdeev, Zh. Eksp. Teor. Fiz. Pis'ma Red. 7, 405 (1968) [JEPT Lett. 7, 318 (1968)]
3. R. J. Taylor, D. R. Baker and H. Ikezi, Phys. Rev. Lett. 24, 206 (1970)
4. S. G. Alikhanov, Zh. Eksp. Teor. Fiz. 60, 982 (1971) [JETP 33, 532 (1971)]
5. A. Y. Wong and R. W. Means, Phys. Rev. Lett. 27, 973 (1971)
6. D. Cohn and K. R. MacKenzie, Phys. Rev. Lett. 28, 656 (1972)
7. K. Saeki and H. Ikezi, Phys. Rev. Lett. 29, 253 (1972)
8. D. W. Forslund and J. P. Freidberg, Phys. Rev. Lett. 27, 1189 (1971)
9. D. Biskamp and D. Parkinson, Phys. Fluids 13, 2295 (1970)
10. R. Z. Sagdeev, Reviews of Plasma Physics (Consultant Bureau, New York, 1969) Vol.IV
11. D. A. Tidman, Phys. Fluids 10, 547 (1967)
12. Y. Kato, M. Tajiri and T. Taniuti, Phys. Fluids 15, 865 (1972)
13. D. W. Forslund and C. R. Shonck, Phys. Rev. Lett. 25, 1599 (1970)

14. R. J. Mason, Phys. Fluids 14, 1943 (1971); 15, 845 (1972)

15. N. Yajima, T. Taniuti and A. Outi, J. Phys. Soc. Japan 21, 757 (1966)

16. P. H. Sakanaka, Phys. Fluids 15, 1323 (1971)

17. R. J. Taylor, K. R. MacKenzie and H. Ikezi, Rev. Sci. Instr. 43, 1675 (1972)

18. H. Ikezi, Y. Kiwamoto, K. Nishikawa and K. Mima, Phys. Fluids 15, 1605 (1972)

19. H. Ikezi and R. J. Taylor, J. Appl. Phys. 41, 738 (1970)

20. H. Ikezi and K. E. Lonngren, to be published.

21. R. J. Taylor and F. V. Coroniti, Phys. Rev. Lett. 29, 34 (1972)

22. T. E. Stringer, Plasma Phys. 6, 267 (1964); B. D. Fried and A. Y. Wong, Phys. Fluids 9, 1084 (1966)

23. P. H. Sakanaka, C. K. Chu and T. C. Marshall, Phys. Fluids 14, 611 (1971)

24. H. L. Berk and K. V. Roberts, Phys. Fluids 10, 1595 (1967)

25. R. C. Davidson, Methods in Nonlinear Plasma Theory (Academic Press, New York, 1972) p.45

26. G. Joyce and D. Montgomery, J. Plasma Phys. 3, Pt.1, 1 (1969)

27. I. B. Bernstein, J. M. Greene and M. D. Kruskal, Phys. Rev. 108, 546 (1957)

28. C. F. MacKee, Phys. Rev. Lett. 24, 990 (1970)

FIGURE CAPTIONS

Fig.1. Plot of electron density (saturated electron current to the Langmuir probe) versus time with distance as a parameter. (a) The case when a density perturbation is applied. (b) The case when the ion-beam is continuously injected and its energy is suddenly increased from 6 volts to 14 volts.

Fig.2. Plot of electron density versus time (top trace) and ion distribution (dot density) in energy-time plane (bottom). The distance from the beam injection point is 12 cm. (A) Background ions in the target plasma. (B) Injected ion-beam. (C) Background ions and reflected ions from the density depression. (D) Ions reflected from the shock front and transmitted through the high density part. (E) High density region.

Fig.3. Pictures of ion distributions for the case where the ion-beam is injected into a low density plasma and the beam energy is instantly increased by 5 volts at $t = 0$. (A) High energy ion beam injected into the target plasma $t \geq 0$. (B) Low energy ion-beam injected into the target plasma $t < 0$. (C) Ions reflected from the potential jump in front of the shock and transmitted through from the high energy beam. (D) Ions reflected from the potential jump in back of shock and transmitted through from the low energy beam as the shock passes. (E) Ions in background plasma. (F) High density region.

Fig.4. Dependence of the shock structure on beam energy, showing two types of shocks and no interacting beam. Time is fixed at 19 μs after the beam injection.

Fig.5. Shock velocity in the center of mass frame (the reference frame moving with the velocity $v_b/2$) and the Mach number as a function of the beam velocity. (a) Experimental results. c_{sE} is the ion-acoustic velocity measured by the propagation of small-amplitude wave. (b) Results of numerical simulations. $c_s \equiv (T_e/M)^{1/2}$. (c) Results of an analysis based on the water-bag model.

Fig.6. Evolution of the ion density $T_e/T_i = 30$, and $v_o/c_s = 1.3$.

Fig.7. Ion-distribution of the shock with time as a parameter. $T_e/T_i = 30$, and $v_o/c_s = 1.3$. (a) $\omega_{pi}t = 10$. (b) $\omega_{pi}t = 40$. (c) $\omega_{pi}t = 70$.

Fig.8. Ion-distribution of the shock with injected beam velocity as a parameter. $T_e/T_i = 30$ and $\omega_{pi}t = 40$. (a) $v_o/c_s = 0.4$. (b) $v_o/c_s = 1.0$. (c) $v_o/c_s = 1.5$ (no shock wave).

Fig.9. Ion-distribution in phase-space and potential profile for "water-bag" analysis.

Fig.10. Plot of V as a function of potential ψ from which the shock solution is obtained.

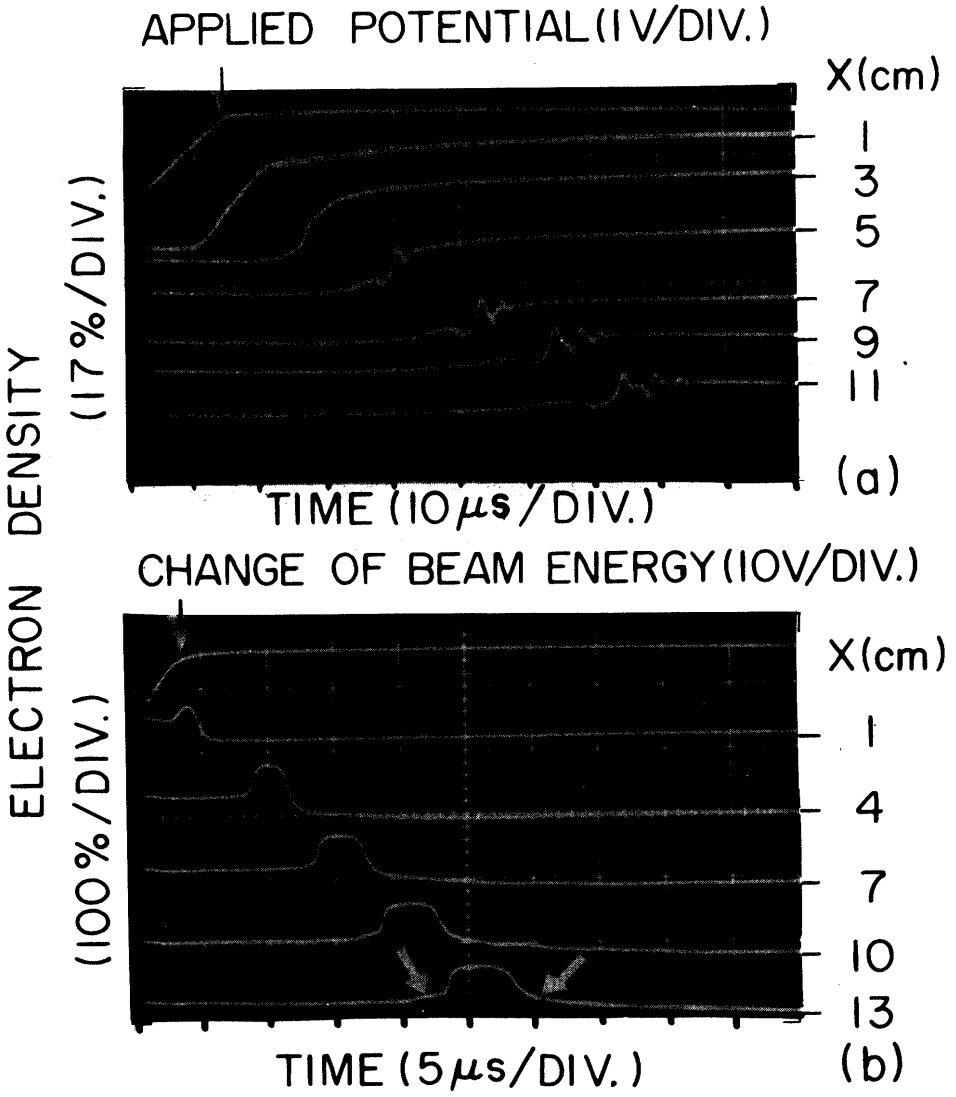
APPLIED POTENTIAL(1V/DIV.)
X(cm)
1
3
5
7
9
11
(a)
ELECTRON DENSITY
(17%/DIV.)
TIME (10μs/DIV.)
CHANGE OF BEAM ENERGY(10V/DIV.)
X(cm)
1
4
7
10
13
(b)
(100%/DIV.)
TIME (5μs/DIV.)

FIG. 1

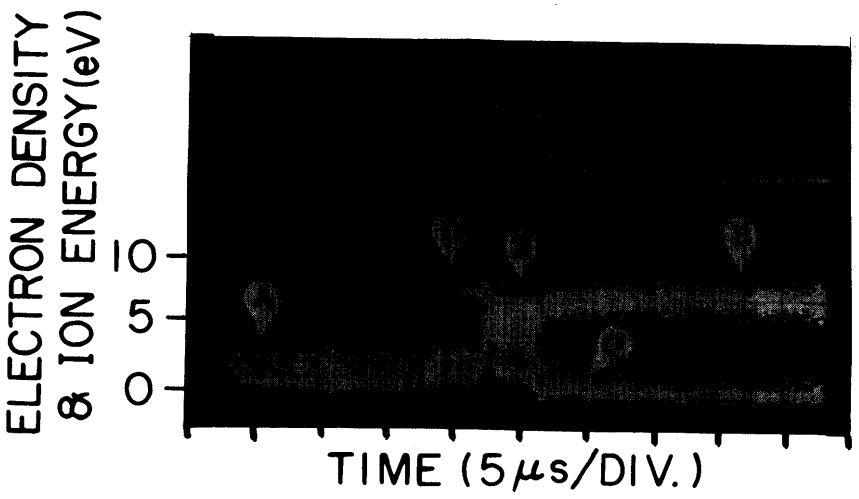

FIG. 2

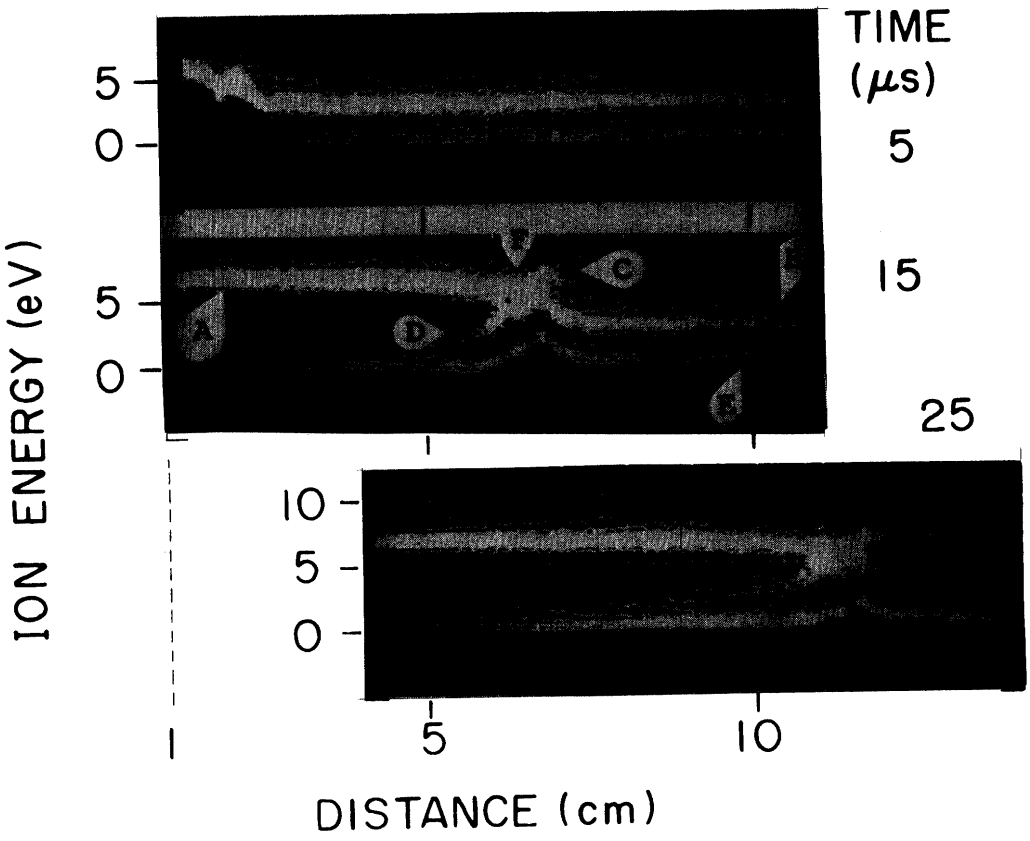

FIG. 3

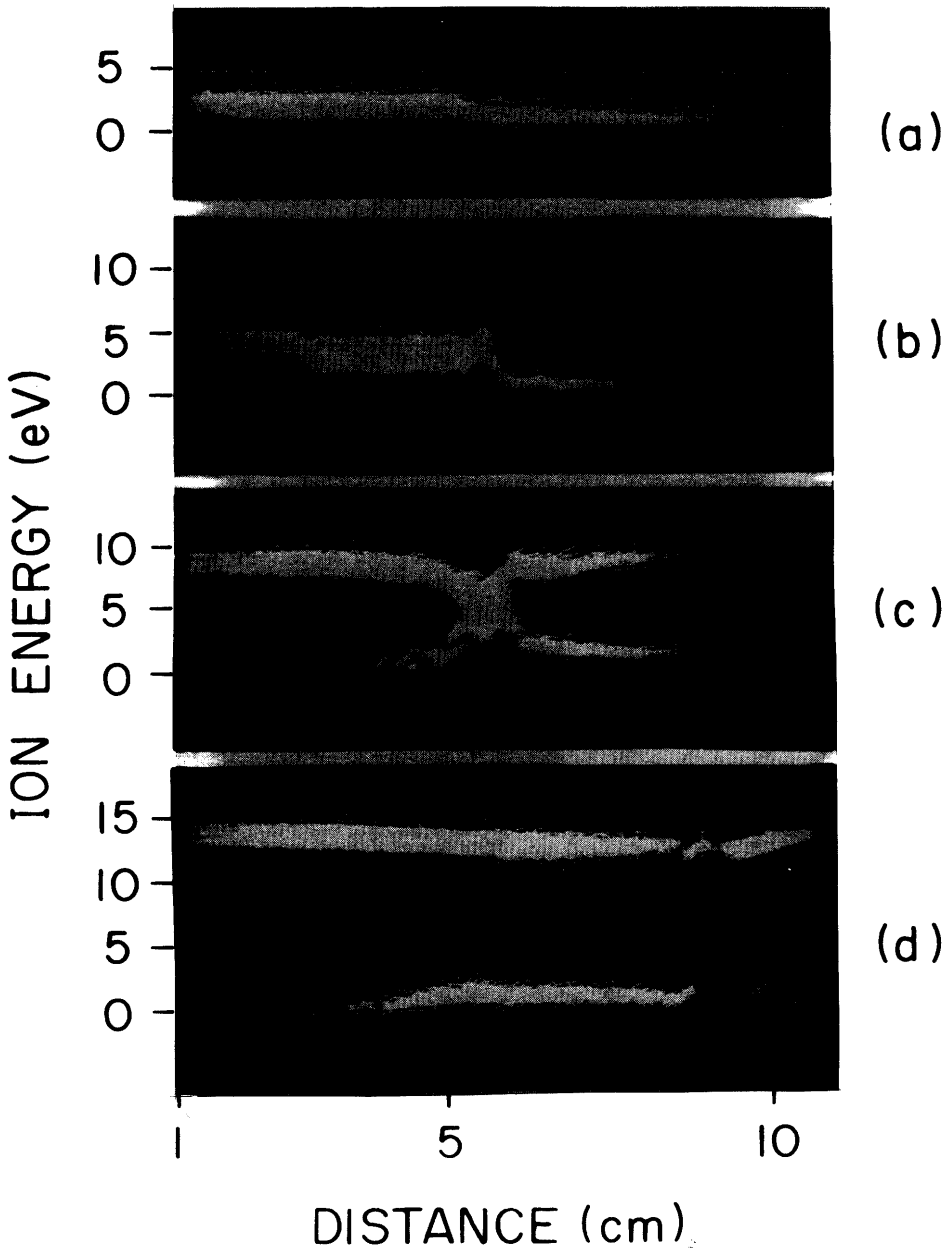

FIG. 4

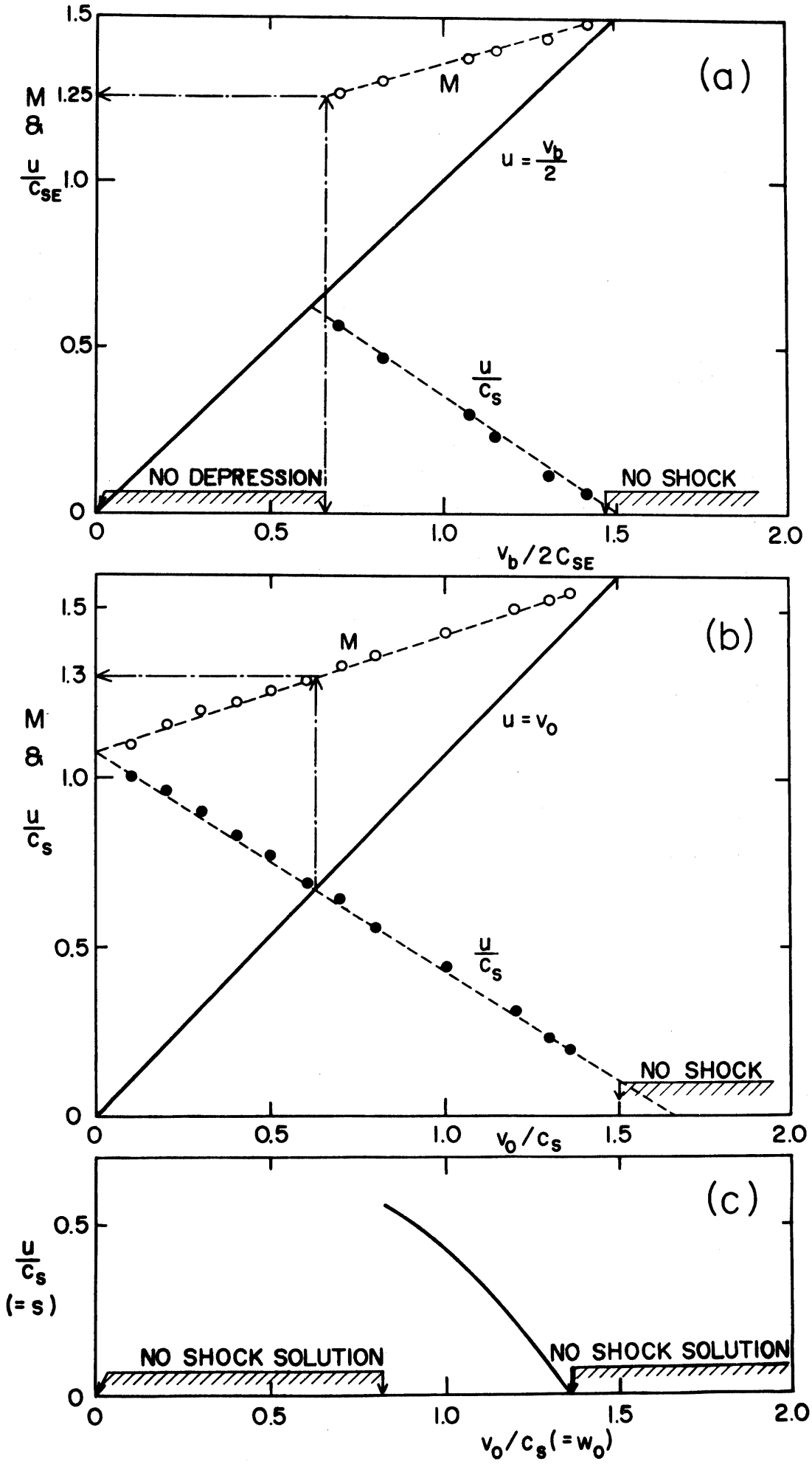
(a)
M
u = v_b/2
u/c_s
NO DEPRESSION
NO SHOCK
M & u/c_SE
v_b/2c_SE
(b)
M
u = v_0
u/c_s
NO SHOCK
M & u/c_s
v_0/c_s
(c)
u/c_s (= s)
NO SHOCK SOLUTION
NO SHOCK SOLUTION
v_0/c_s (= w_0)

FIG. 5

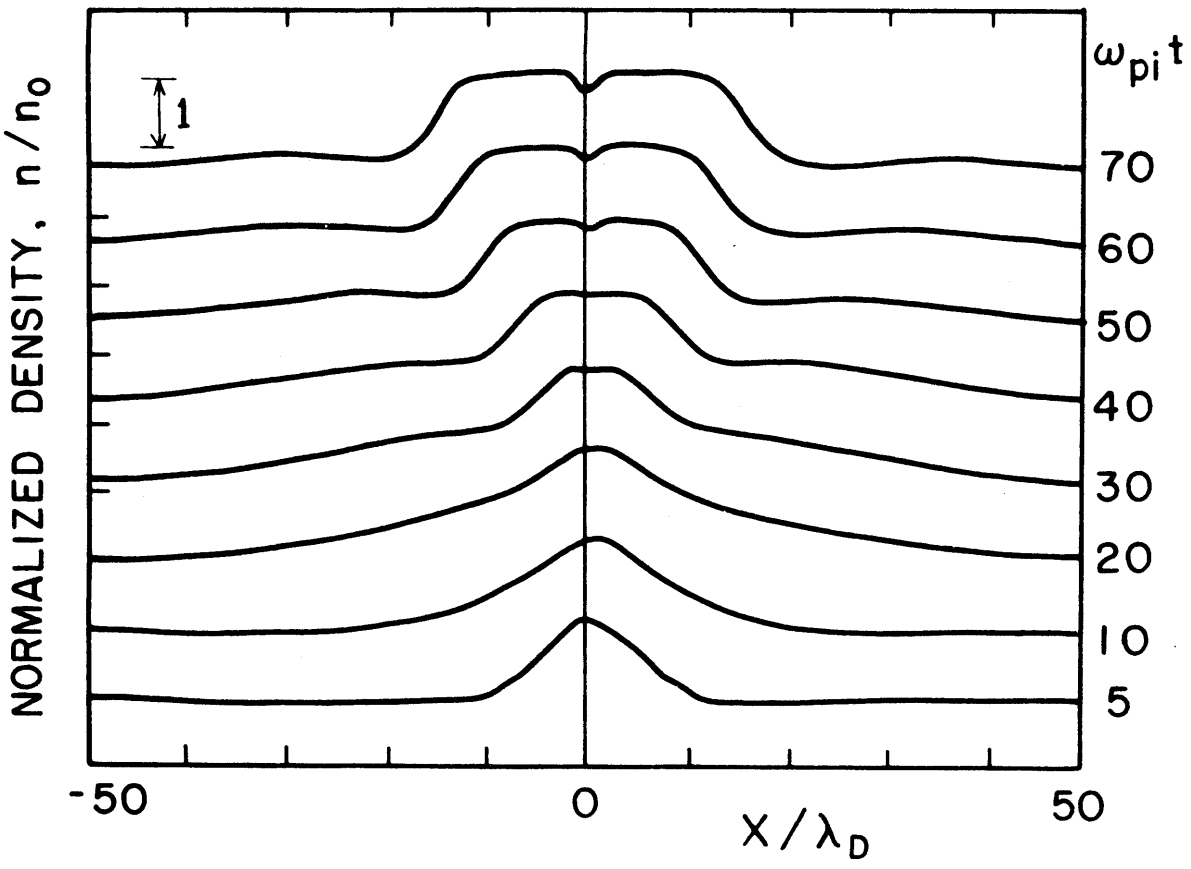

FIG. 6

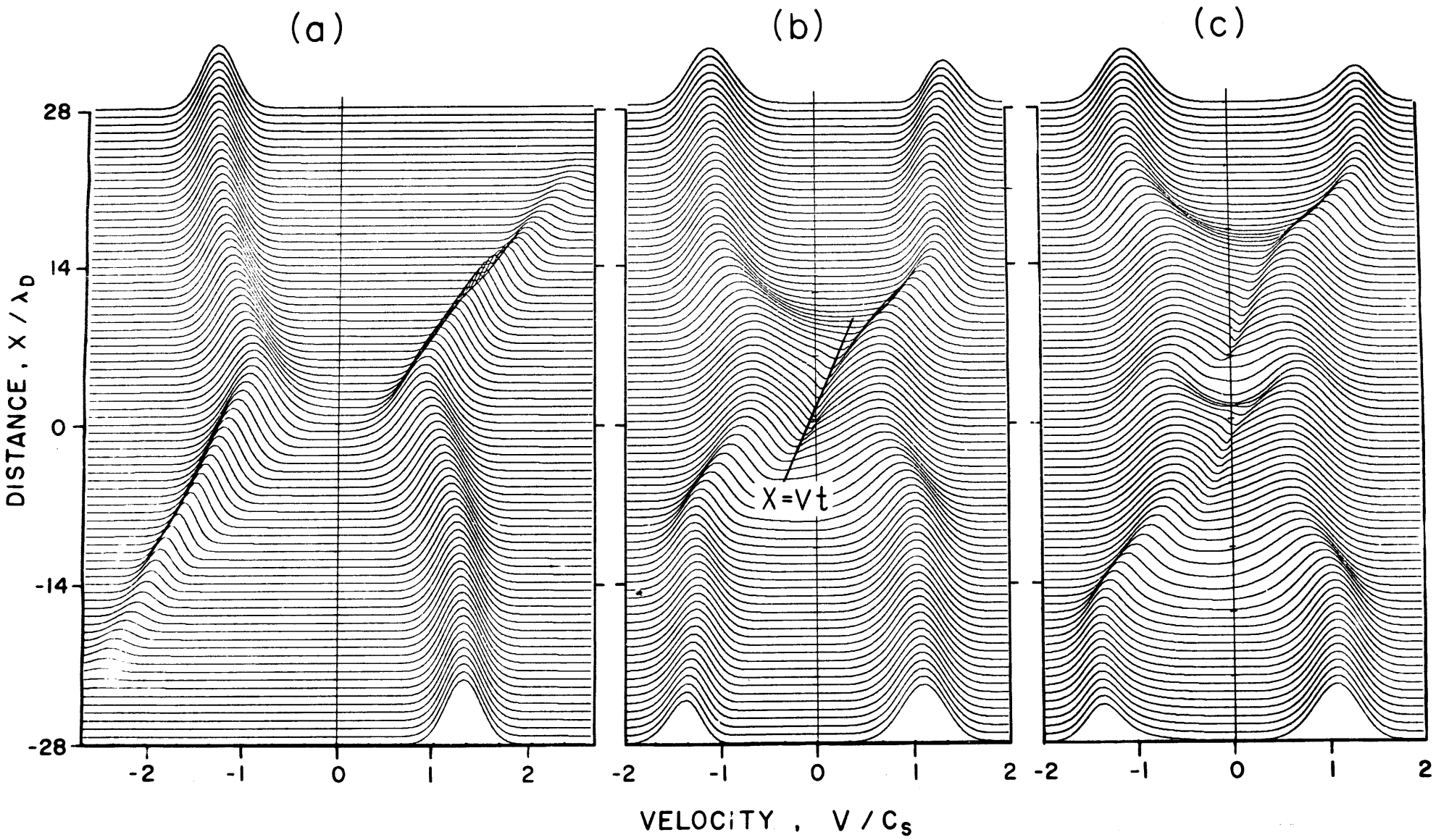

FIG. 7

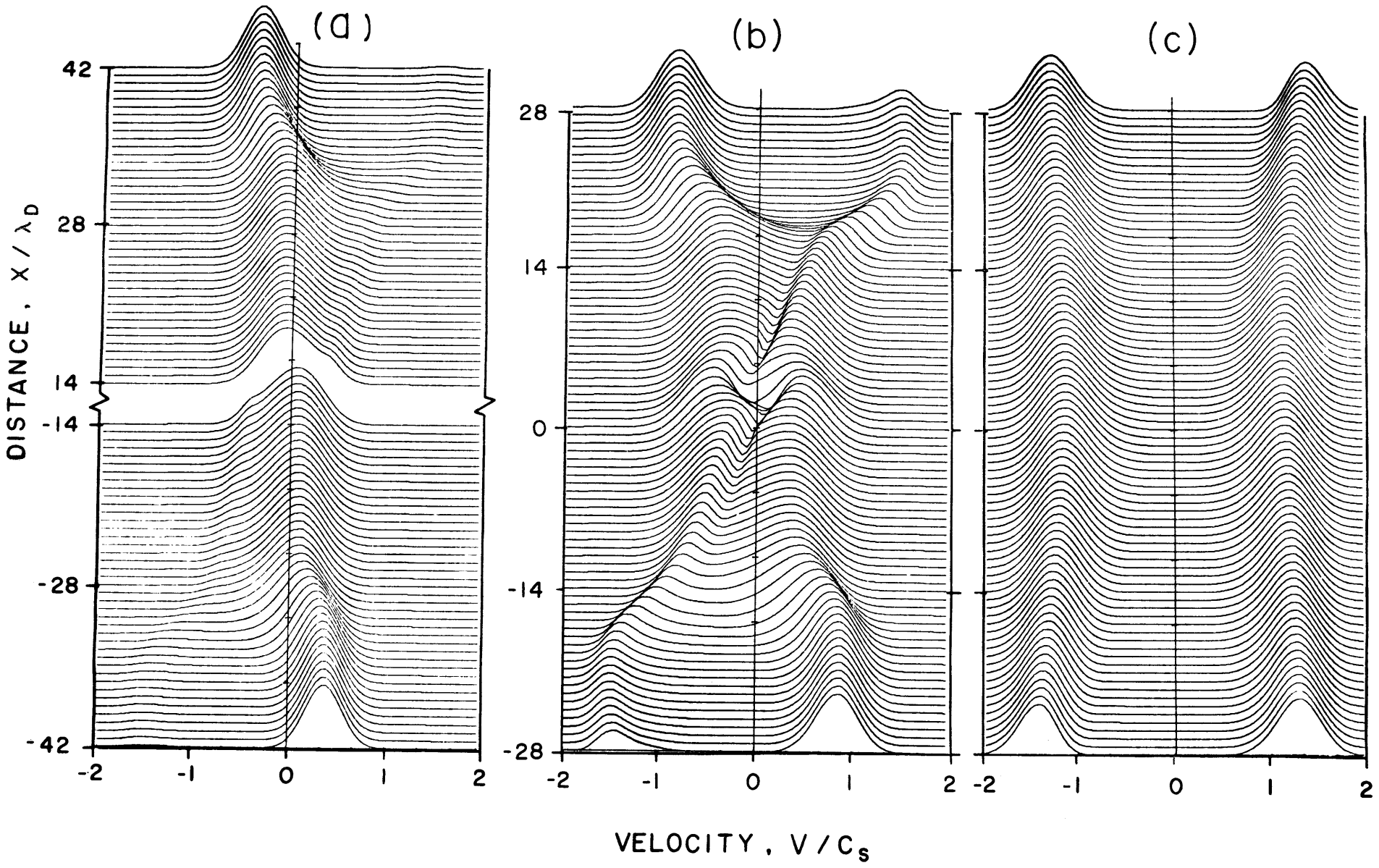
(a)
(b)
(c)
42
28
14
-14
-28
-42
28
14
0
-14
-28
-2
-1
0
1
2
DISTANCE, X / λD
VELOCITY, V / Cs

FIG. 8

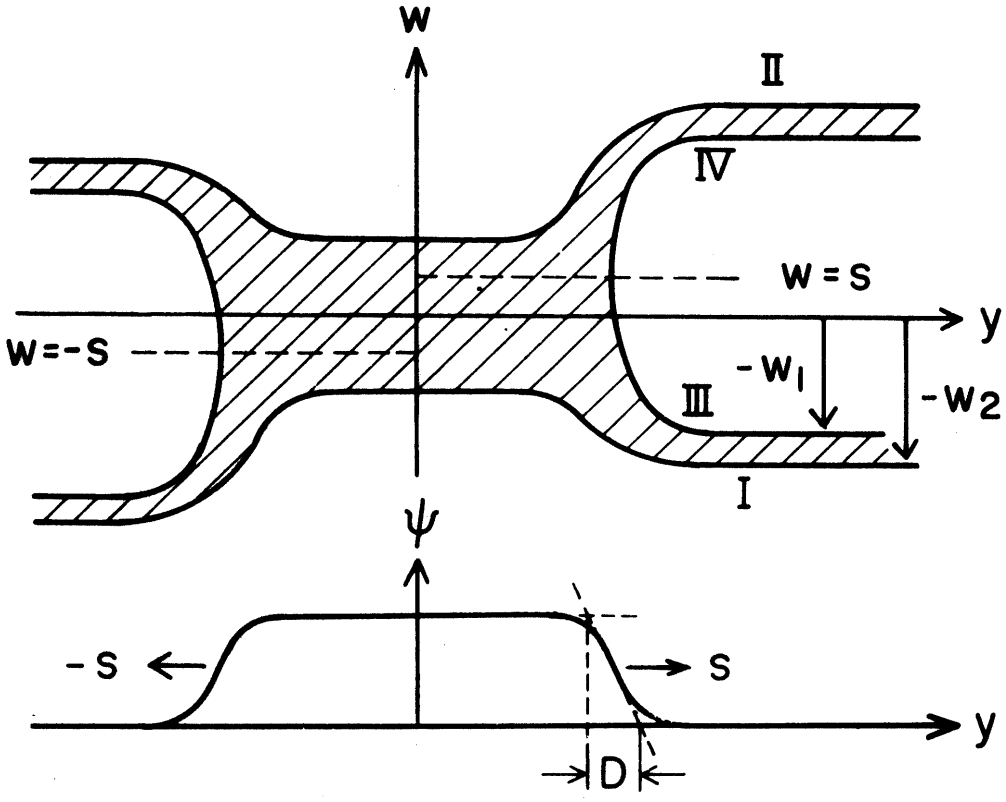

FIG. 9

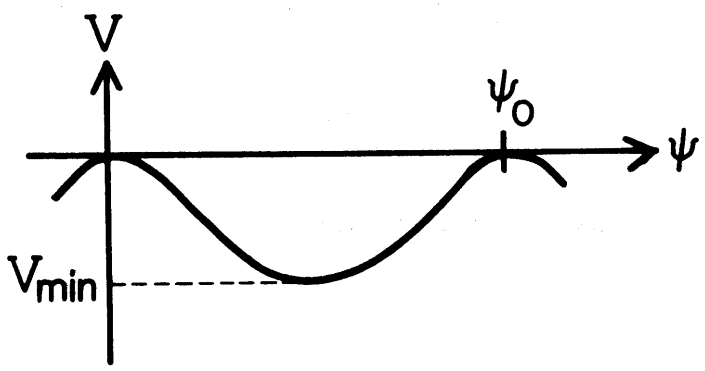

FIG. 10